



Iranian Research Organization
for Science and Technology
(IROST)

Advances
Environmental
Technology



Journal home page: <https://aet.irost.ir/>

An experimental study on the effect of composite electrode on the membrane- assisted electrode in CDI and MCDI processes towards nitrate ion selectivity

Reza Fatemina ^a, Soosan Rowshanzamir ^{a,b,c,*}, Foad Mehri ^d

^a School of Chemical Engineering, Iran University of Science and Technology, Narmak, Tehran, Iran

^b Fuel Cell Laboratory, Green Research Center, Iran University of Science and Technology, Narmak, Tehran, Iran

^c Center of Excellence for Membrane Science and Technology, Iran University of Science and Technology, Narmak, Tehran, Iran

^d Faculty of Engineering Modern Technologies, Amol University of Special Modern Technologies, Amol, Mazandaran, Iran

ARTICLE INFO

Document Type:
Research Paper

Article history:
Received 24 May 2022
Received in revised form
30 July 2022
Accepted 30 July 2022

Keywords:
Selective nitrate removal
Electrosorption
Composite electrode
Membrane capacitive
deionization

ABSTRACT

The removal of nitrate concentrations above international drinking water standards is a prominent task of governments. In this regard, various technologies such as reverse osmosis, biological denitrification, electro dialysis, and capacitive deionization (CDI) as an electrochemical approach have been used for nitrate removal from water. In the present research study, a novel composite electrode named E2 was synthesized and used to improve the efficiency of the membrane capacitive deionization (MCDI) process for increasing the electrosorption capacity of nitrate from water. E1 as a based electrode composed of activated carbon (AC), PVDF, and E2 as an optimal electrode containing (AC), PVDF, ZrO₂, and PANi -ES were utilized. The morphology and structure of the composite electrode were determined using field emission scanning electron microscopy (FESEM), Brunauer-Emmett-Teller (BET), Fourier-transform infrared spectroscopy (FTIR), X-ray diffraction (XRD), and energy-dispersive X-ray spectroscopy (EDAX) techniques. Also, the cyclic voltammetry (CV) and electrochemical impedance spectroscopy (EIS) methods were applied to investigate the electrochemical behavior of the electrodes. In the MCDI process with the presence of the E2 electrode, the amounts of separated nitrate ion and its adsorption efficiency were 7.51 mg/g and 81.6%, respectively; this demonstrated that the capacity of the adsorbed nitrate ion by the MCDI process was 30.34% higher than the CDI process. On the other hand, the E2 electrode, compared to the E1 electrode, ameliorated the performance by almost 50% of the amount of adsorbed nitrate ion and also ion adsorption efficiency during the CDI and MCDI processes.

*Corresponding author: Tel: 982177491242

E-mail: : rowshanzamir@iust.ac.ir

DOI:10.22104/AET.2022.5661.1543

1. Introduction

Nowadays, the global application of the CDI process for desalination of brackish water with more efficient performance than existing technologies is increasing [1]. Additionally, its application has recently been extended to water pollutant treatment processes such as fluoride [2], nitrate [2], sulfate [3], heavy metals, and ions [4-6]. This method is based on electrosorption within at least a pair of porous electrodes or an ion-exchange membrane in an electrochemical cell by a working voltage range of (1.2-1.5) V [7]. However, an applied potential of up to 2.0 V has been reported due to the voltage drop in a cell regarding the overall cell resistance [8-9]. This technology has attracted much attention due to its advantages: low energy consumption, environmentally friendly, easy operation, adsorption of a large range of ions with a high separation rate, and no high-pressure pump required [10-12]. Nevertheless, problems such as non-selective ion adsorption and the simultaneous occurrence of the adsorption-desorption cycle during the regeneration of the electrode in a conventional CDI process lead to higher energy consumption, decreasing the electrosorption capacity and ion adsorption efficiency [13-14]. Therefore, various efforts have been carried out to overcome these problems, including the incorporation of an ion-exchange membrane in the MCDI process as an improved configuration of the CDI process. In the MCDI process, an anion-exchange membrane (AEM) and a cation-exchange membrane (CEM) are placed in front of the anode and cathode, respectively. The presence of charged groups, such as quaternary ammonium cations (NH_3^+) in the AEMs, results in the selective migration of ions of opposite charge (counter-ions) and blocks the transport of ions of the same charge (co-ions), thereby increasing ion removal efficiency. These charged materials occur either naturally in the polymers or can be bonded into the membrane matrix through chemical processes. These charged materials occur naturally in the polymers or can be bonded in the membrane structure through chemical processes. [15]. Also, based on the membrane type, it can act selectively in the adsorption of ions [16]. Although the

performance of MCDI is considerable in comparison with CDI, the cost of the membrane may hinder its usage on an industrial scale. So, there is a vast majority of research to synthesize appropriate ion-selective electrodes [17-18]. All electrodes used in this process were required to have some key properties, including high specific surface area, high adsorption capacity, good porous structure, high electrical conductivity, and suitable wettability [19-20]. Different forms of carbon materials with a porous structure such as AC [21], carbon black [22], carbon aerogels [23], carbon nanotube [24], nanofiber [25], graphene and its composites [26-27] can usually be used as the CDI electrodes. Some metal oxides and conjugated polymers have been used efficiently to achieve these desired properties [24]. For example, the combination of metal oxide nanoparticles such as ZrO_2 and MnO_2 in some carbon materials can improve the specific capacitance of the electrode [28-29] as well as the ion adsorption capacity in the CDI system. In the case of ion-selectivity, the presence of imine and amine functional groups in the electrode can increase the affinity of the electrode toward nitrate ions [30]. In this way, some advantageous materials, such as nitrogen-containing ones like polyaniline (PANI) [31-32] and nitrogen-doped activated carbons, can be used to improve nitrate selectivity adsorption and applied in the CDI process. In another work, the removal of nitrate from the mixed-salt feed solution in a three-electrode system by carbon electrodes coated with $\text{SiO}_2\text{-Al}_2\text{O}_3$ was investigated, and higher nitrate removal was obtained compared to the uncoated carbon electrodes [31]. Hu et al. (2018) [32] introduced a new electrode by doping Pd nanoparticles into NiAl-LMO enriched electron transport in the electrode sheet to separate nitrate from water. The Pd/NiAl-LMO as a CDI electrode could preferentially adsorb nitrate ions to attain an ion removal efficiency of approximately 47.43%. Besides the electrodes, commercial ion-selective membranes are usually used in the MCDI process to improve the performance of the CDI process to remove ions selectively (e.g., nitrate ion) from water [33]. Kim et al. [34] demonstrated the removal of nitrate ions from the binary salt feed solution using a commercial anionic membrane

(Neosepta AMX membrane, Astom Co., Japan) with a carbon electrode made of AC and PVDF through the MCDI process. The results revealed that the fraction of adsorbed nitrate ions was in the range of a minimum of 31.7% to a maximum amount of 41.0%, depending on the applied current. Tang et al. (2015) [2] utilized a pilot CDI unit (Aqua, EWP company, USA) in batch- mode for studying the removal efficiency for nitrate in the various initial NaCl and NaNO₃ concentration amounts. Baghodrat et al. (2020) [35] synthesized an anionic membrane containing a quaternary amine functional group with a combination of an AC/PVDF electrode. They investigated its performance through the MCDI process to remove nitrate ions selectively from the feed solution. In the previous study [36], the percentage of adsorbed nitrate ions was estimated at about 59%. In another work, Kim et al. (2020) [37] utilized an activated carbon electrode coated with an IX polymer containing selective A520E resin to enhance selective NO₃⁻ adsorption in the feed solution during the MCDI process. The selectivity of nitrate ions compared to other anions was reported at 1.35. Nitrate selective membranes usually contain amine and quaternary ammonium functional groups in their backbone [39-40]. Although, using an ion-selective membrane along with electrodes can significantly enhance the removal efficiency of special ions in the process, their cost is relatively high, and the available active area is limited to their apparent surface area. On the contrary, various research has taken advantage of the merits of some key characteristics of ion-selective electrodes, such as higher wettability and porosity and also lower resistance [41-42]. Based on other research, ion-selective electrode or ion-exchange selective membranes have been used individually, while a simultaneous combination of both membranes could synergistically enhance the performance of the ions. Furthermore, a few studies were allotted to compare and disclose the nitrate ion-selectivity of the modified electrode with that of the membrane-assisted electrode through CDI vs. MCDI [38], [43]. Therefore, in this paper, the purpose is not only to investigate and compare the nitrate ions adsorption behavior by a novel nitrate ion-selective composite electrode in CDI and MCDI process but also to enhance the

nitrate ion adsorption capacity and removal efficiency by combining nitrate-ion selective electrode and ion-exchange membrane.

2. Material and methods

2.1. Materials

The activated carbon (BET surface area of 787 m²/g), N-methyl-2 pyrrolidone (NMP), and ethanol (99.95%) were bought through Merk Co., Germany. The Polyaniline-emeraldine base (PANI-EB) (MW of 20,000 g/mol) and Polyvinylidene fluoride (PVDF, MW of 530,000) were purchased from Sigma-Aldrich Co. Ltd. The nanoparticle of ZrO₂ was provided by US Research Nanomaterials, Inc., USA. The graphite sheets (500 μm thickness) were purchased from Dongbang Carbon Co., China. An anion exchange membrane (fumasep® FAB-PK-130) was supplied by Fumtech BWT GmbH, Germany. All the chemical materials were of analytical grade and applied without extra purification.

2.2. Fabrication of composite electrode

The manufacture of the optimal electrode was performed by the ex-situ polymerization method [43]. This method is a solution processing technique that generally consist of mixed solutions of AC, PVDF, ZrO₂, and PANi-ES. The fabrication details of the composite electrode have been thoroughly described in our previous paper [36]. In brief, Because of inadequate electrical conductivity of the PANi-EB material, it was converted to the emeraldine salt of polyaniline (PANI-ES). So, the PANi-ES could attain the high electrical conductivity using the chemical technique in the presence of hydrochloric acid. (See Figure 1). The locations of imine, as a functional group or chemical compound containing a carbon-nitrogen double bond (C=N), in the EB form of polyaniline are easily protonated by duplication and significantly increase the conductivity and produce positive charges in the polymer network [46-47].

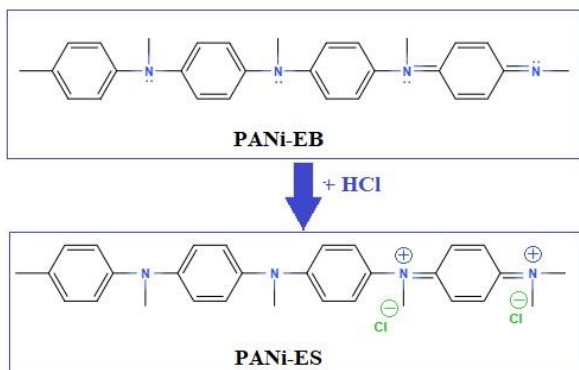


Fig. 1. The converted of EB-PANi form to ES-PANi.

The AC, PVDF as a binder, ZrO_2 nanoparticle, and PANi- ES powder material were mixed exclusively in NMP solvent by a magnetic stirrer in the three different Erlenmeyer flasks for 24 h to manufacture the carbon composite electrode sheets. Then, the substances of all the flasks were poured to another container, and the solution was mixed again for 24 h to have homogenized carbon slurry. Next, the solution was covered on the graphite sheet (as a current collector) using a casting knife applicator and dried in an ordinary oven at $55^\circ C$ for 14 h to form a composite carbon electrode sheet. To ensure the absence of NMP solvent in the electrode structure, the composite electrode plates were again dried in a vacuum oven at $55^\circ C$ for 3 h. The thickness of the carbon layer on the graphite sheet was measured at $215.0\ \mu m$. According to our previous work, the optimal composite electrode was named the E2 electrode, while the E1 electrode, as the basic electrode, was prepared according to the formulation used in the references [34]. The elements and their percentage of the E1 and E2 electrodes are indicated in Table 1.

Table 1. The components of the E1 and E2 electrodes.

Electrode	AC (wt %)	PVDF (wt %)	ZrO_2 (wt %)	PANi-ES (wt %)
E1	90.0	10.0	0.0	0.0
E2	80.0	8.0	6.0	6.0

2.3 Chemical/physical characterization

The morphology of the E1 and E2 composite electrodes was characterized by FESEM (TESCAN, Czech Republic). The specific surface area and mean pore diameter were determined by the BET method using a Belsorp system (BEL Japan, Inc.). The FTIR technique (Thermo Electron Scientific Instruments LLC, USA) was used to identify the

functional groups in the composite electrode, XRD analysis (Philips X'Pert, Netherlands) gave information about the crystallographic structure, and the EDX method (TESCAN, Czech Republic) determined the chemical composition and the elemental analysis of the E2 electrode.

2.4 Electrochemical characterization

The cyclic voltammetry (CV) technique was applied to measure the specific capacitance of the electrodes in the CDI process [46]. Usually, a rectangular voltammogram in the current-voltage plot demonstrates the high electric-double-layer capacitance of the electrodes, and the plots with the absence of redox peaks show that the faradaic process did not occur [9]. The electrochemical impedance spectroscopy (EIS) and CV tests were performed in a 1.0 mol/L $NaNO_3$ solution by a conventional three-electrode system with the carbon composite coated on a graphite sheet ($1.0\ cm^2$) as a working electrode, platinum (Pt) plate as a counter electrode ($3.0\ cm^2$), and Ag/AgCl in KCl saturated as a reference electrode at room temperature. The applied potential range and scan rate were -0.4 to $0.6\ V$ [versus Ag/AgCl] and $10\ mV/s$, respectively. The EIS test was accomplished in the frequency range from $100.0\ kHz$ to $10.0\ mHz$ using the above cell, and the amplitude of the alternating potential was $10.0\ mV$ around the equilibrium potential ($0.0\ V$). An SP-150 potentiostat (Bio-Logic Science Instruments SAS, France) was utilized as a supplier of applied voltage in all measurements. The specific capacitance (C_s , (F/g)) of the composite electrode was calculated by the I-V diagram and using Eq. (1) [47]:

$$C_s = (I_a - I_c) / 2\nu m \quad (1)$$

where ν is the experiment's scan rate (V/s), m is the total mass of the electrodes (g), and I_a and I_c are the anodic and cathodic currents (A), respectively.

2.5 Experimental set-up

The CDI and MCDI experimental systems both consisted of a feed tank, a peristaltic pump (Lab 2015, Baoding Shenchen Precision Pump Co. Ltd., China), a conductivity meter, and a pH meter (Figure 2). The CDI module contained two similar electrodes (E2 optimal electrodes) with an effective area of $25\ cm^2$ that was separated by a polymer

mesh spacer with the thickness of 250 μm . The MCDI cell was the same as the CDI cell, except that an AEM (fumasep® FAB-PK-130, Fumatech BWT GmbH, Germany) was attached to the carbon-

based electrode having a positive charge when the power was applied. The Fumasep FAB-PK-130 is a PK reinforced AEM with high selectivity and mechanical stability [48].

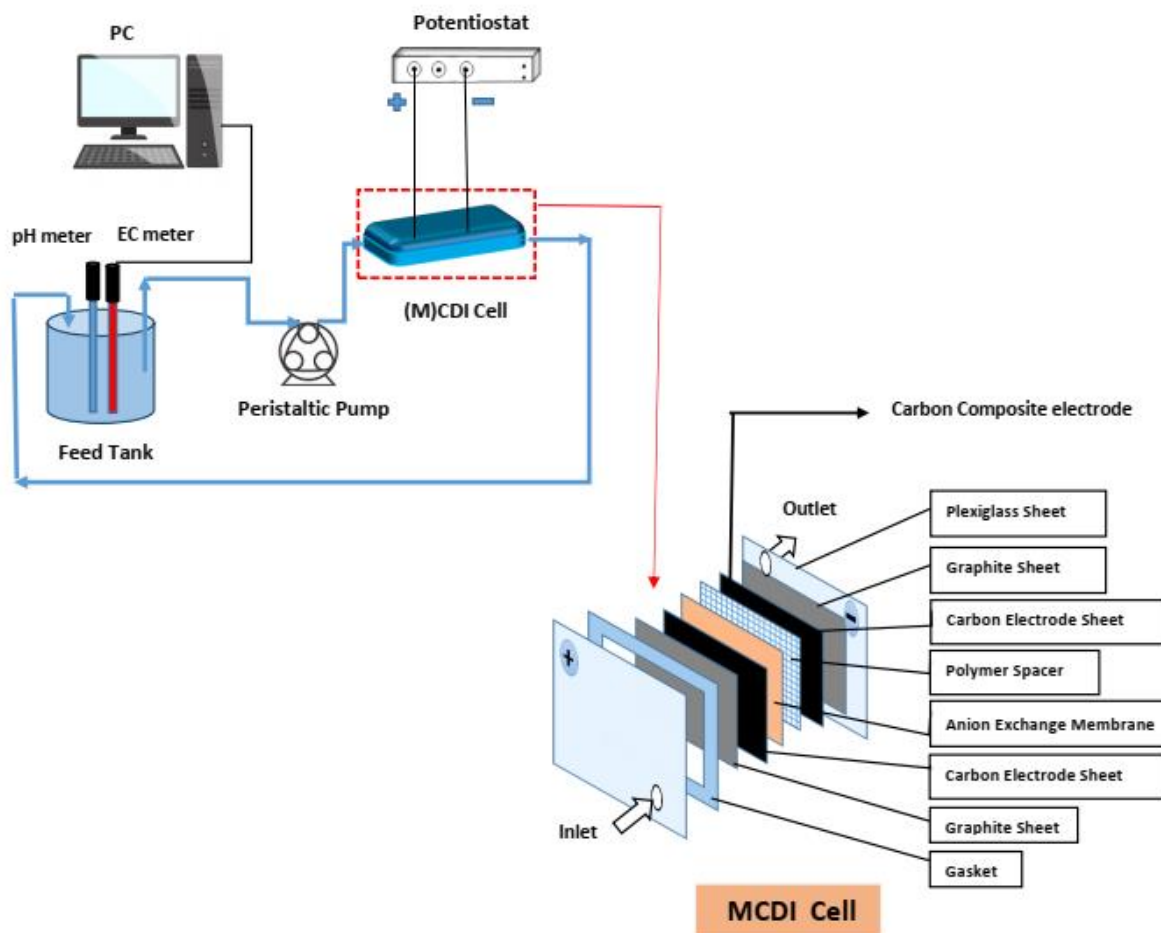


Fig. 2. Schematic diagram of (M) CDI configuration in batch mode.

In this study, the aim was to remove nitrate ions, and only an AEM was used in the MCDI cell. Therefore, the cation exchange membrane was not applied to adsorb sodium cations because there was no cation competing with it in the feed solution. The apparent area of each electrode, AEM, and spacer in the (M) CDI cell was $5 \times 5 \text{ cm}^2$. Indeed, no significantly different condition was applied between the CDI and MCDI cells. The characteristics of the composite electrode and the AEM are summarized in Table 2. To remove ions from the electrolyte solution, a direct voltage of 2.0 V was applied between the composite electrodes, and the flow rate and pH of the feed solution were 10 ml/min and 6.0, respectively. A mixed solution was prepared using a binary salt solution of NaCl and NaNO_3 with an initial concentration of 100 mg/L. The batch experiments were performed at

room temperature using a 0.985 g mass of electrodes and 200 mL of the feed solution. The shift change within the conductivity of the feed tank solution and its pH was evaluated during the adsorption and desorption cycle using a conductivity meter (EC-470L, istek, inc., Korea) and a pH meter (P25, istek, inc., Korea). The conductivity meter was connected to a computer for measuring the changes in the solution electrical conductivity every three seconds. The amounts of the adsorbed ions were calculated by measuring the ion concentration in the inflow and outflow of M(CDI) cell during the adsorption and desorption cycle using an ion chromatography device (Sykam GmbH, Germany) with an SI-52 4E column (Shodex). Additionally, the changes in the chloride and nitrate ion concentrations were measured by periodically withdrawing samples. A DC

potentiostat (SP-150 potentiostat, Bio-Logic Science Instruments SAS) was applied to supply the voltage. In the current study, the adsorbed ion capacity (E_c , mg/g), the adsorbed ion efficiency (η_i), and nitrate ion selectivity ($S_{NO_3^-}$) were calculated using the following equations [8], [51]:

$$E_c = (C_i - C_f) \cdot V/m \quad (1)$$

$$\eta_i = [(C_i - C_f)/C_i] \times 100 \quad (2)$$

$$S_{NO_3^-} = \eta_{NO_3^-} / \eta_{Cl^-} \quad (3)$$

where C_f (mg/L) and C_i (mg/L) are the final and initial concentrations of $NaNO_3$ and $NaCl$ (or Na^+ , Cl^- and NO_3^- ions) in (M)CDI process, respectively. V (L) is the volume of the feed, and m (g) is the sum of the electrodes mass. The ion concentrations were measured by an ion chromatography system.

Table 2. Main characteristics of the composite electrode and the AME used in (M)CDI process.

Main characteristics	Value
Carbon-based Electrodes	
Mass of electrodes (g)	0.985
Thickness (μm)	215
Surface area (m^2/g)	177.7
Mean pore diameter (nm)	5.64
Specific Capacitance (F/g)	58.67
Anion Exchange Membranes	
Type	fumasep® FAB-PK-130
Color	Brown
Thickness (μm)	140
Ion exchange capacity (in Cl^- form), meq/g (dry)	1.0
Membrane area resistance (in Cl^- form), $\Omega \text{ cm}^2$	9.0
pH stability range at 25° C	0-14

3. Results and discussion

3.1. Morphology of the AC / PANi / ZrO_2 electrode

Figure 3 shows the SEM images of the E1 and E2 electrodes, respectively. In the SEM image of the E1 electrode (Figure 3a), the suitable distribution and positioning of the PVDF particles as a binder agent in the electrode are observed. The PVDF in the carbon electrode is present as separated irregular-

rough particles that interconnect the carbon powders, which causes the enhancement of the mechanical strength of the electrode. However, using binders in the electrode preparation decreases electrical conductivity and consequently affects its performance [50]. This issue has been addressed by incorporating PANi-ES as a conducting polymer in the composite matrix. The ZrO_2 nanoparticles are incorporated into the activated carbon, which results in a network structure that diminishes the particle agglomeration [18]. The distribution of PANi and ZrO_2 nanoparticle components in the carbon matrix structure of the E2 electrode causes a network structure in the electrode with a particle size from 25 nm to 51 nm in Fig. 3b. Therefore, ZrO_2 and PANi contribute to enhancing electrosorption by modifying surface area as well as the wettability and electrical conductivity of the E2 electrode [53-54].

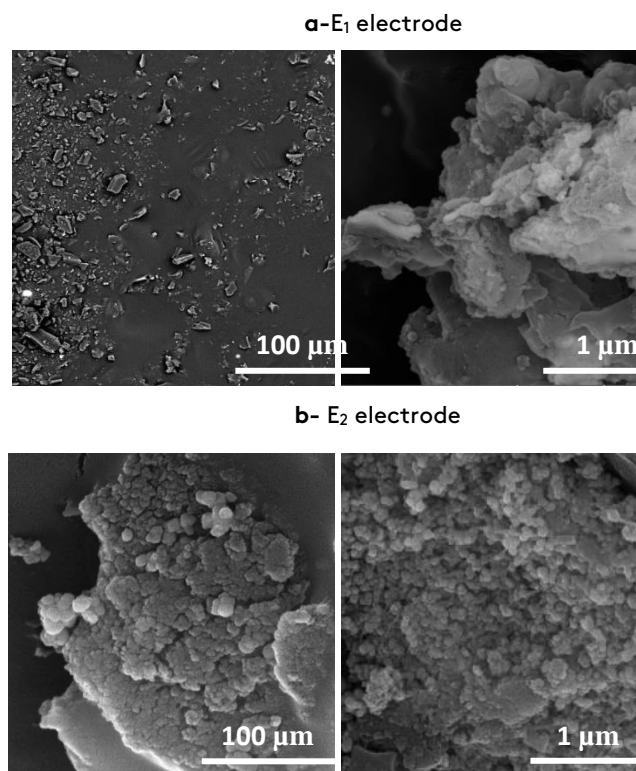


Fig. 3. SEM images of E1 and E2 composite electrodes.

3.2. Porosity analysis

Nitrogen adsorption-desorption isotherms of both the E1 and E2 electrode materials are presented in Figure 4. As shown in Figure 4, the isotherms exhibit a standard type IV, with the existence of a hysteresis slope at higher relative pressures,

indicating the presence of macroporosity and mesoporosity with narrow slit-like pores [53]. The adsorption isotherm of E2 demonstrated an increment in N₂ adsorption at the low relative pressure area ($P/P_0 < 0.05$), indicating the existence of micropores. Moreover, the E2 electrode demonstrated a further ($P/P_0 > 0.05$) steep increase in N₂ uptake compared to the E1 electrode, which shows the presence of larger mesopores.

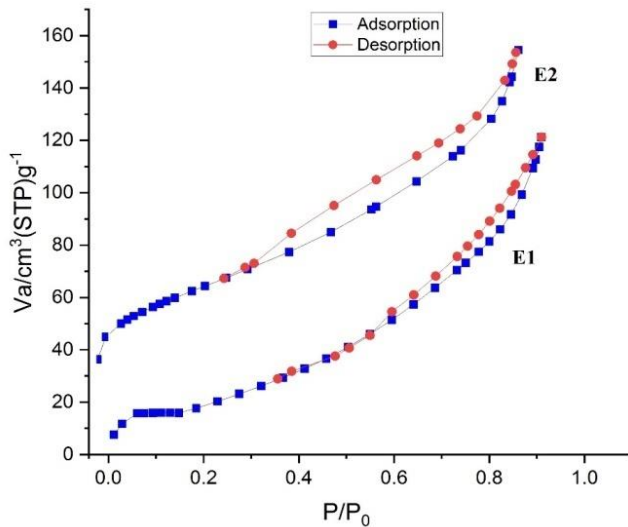


Fig. 4. N₂ adsorption-desorption isotherms of both E1 and E2 electrodes.

The BET specific surface area was 142 m²/g and 177 m²/g for the E1 and E2 electrodes, respectively, which indicated that the surface area of the E2 electrode was 24.64 % higher than the E1 electrode. According to the pore size distribution of the electrodes in Figure 4, it is found that the E2 electrode includes more portion of micropores and mesopores than the E1 electrode, which is supposed to be optimum for electrosorption in CDI and MCDI

processes [56-57]. The presence of ZrO₂ and PANi in the E2 electrode structure could provide accessible active sites by overcoming the van der Waals interaction between AC particles for agglomeration [43]. The decrease in N₂ adsorption capacity by the E1 electrode and the reduced number of mesopores compared to E2 might be due to the blocking of the porosity of the pristine AC by a polymeric binder [56]. Although the micropores contributed to enhancing the specific surface area of the electrodes, they are hardly available for the ions, so they would decrease the specific surface area [59-60]. This is because the E1 electrode lacks good wettability and high electrical conductivity. Indeed, the wettability of electrolytes on the electrode surface is regarded as a significant subject to expand the effective surface area and enhance the specific capacitance [59].

3.3. FTIR analysis

In Figure 5a, C–O stretching vibration peaks appear at approximately 1103 cm⁻¹, 1637 cm⁻¹ is related to the C=C bond, and 3433 cm⁻¹ is attributed to the O–H stretching vibration [52]. In Fig. 5b, as the spectrum of the E2 composite electrode, peaks related to the C=C stretching in quinoid and benzenoid forms turn out at 1566 and 1473 cm⁻¹, respectively [31-32], [62]. The peak at 2925 cm⁻¹ is responsible for the terminal quinoid–N–H stretching of PANi-ES, and the peak at 3443 cm⁻¹ returns to the O–H stretching vibration. The peak at 792 cm⁻¹ belongs to the characteristic peaks of ZrO₂ [63]. Therefore, the existing functional groups in the spectrum of the E2 electrode demonstrate the successful mixing of PANi and ZrO₂ into the carbon matrix.

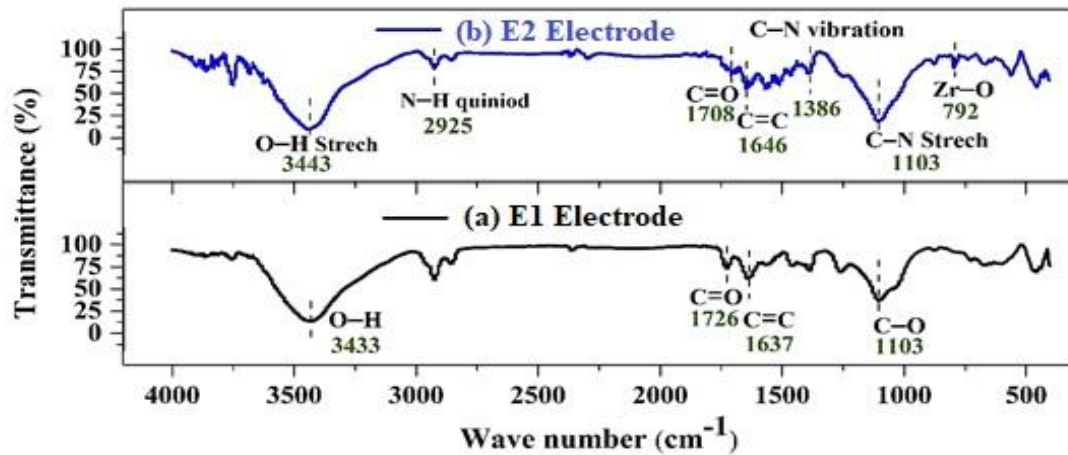


Fig. 5. FTIR spectra of E1, and E2 electrode.3.4.

3.4. XRD analysis

The XRD test is a non-destructive method that gives precise data about the crystallographic structure, physical properties, and chemical composition of nanocomposites. [64]. Figure 6 shows the XRD patterns of ZrO_2 , emeraldine salt PANI, and E2 electrode. In Figure 6a, the XRD pattern of ZrO_2 shows two strong and sharp diffraction peaks at $2\theta = 28.5^\circ$ and 32° , which indicate a crystalline structure. A small and wide peak exhibited in the region of $2\theta=23.5^\circ$ in Figure 6b is a benchmark for ES-PANI. Polyaniline has semi-crystalline structures as the result of polymer chains, which are kept along alternately parallel and vertical, and its crystalline part is surrounded by amorphous regions [64].

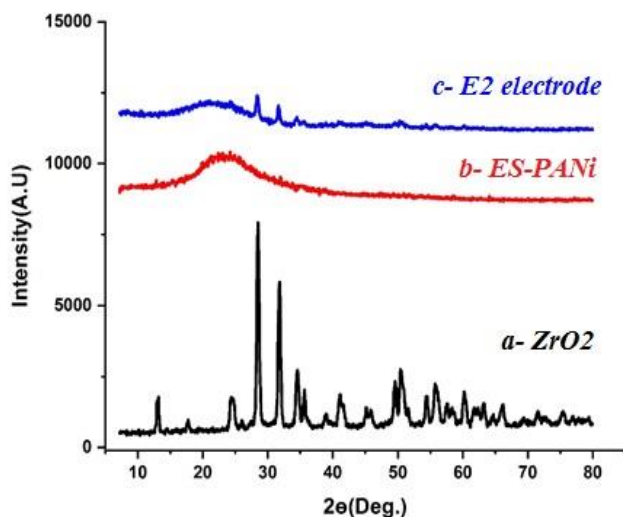


Fig. 6. The XRD pattern of the E2 composite electrode.

The XRD pattern of the E2 composite electrode is a combination of the X-ray diffraction patterns of ES-PANI and ZrO_2 materials with attenuated peaks, as shown in Figure 6c. In this pattern, the ES-PANI peak shifts from 23.5° to 22° , while the ZrO_2 peaks are weakened but with almost no displacement. These changes in the XRD pattern of the E2 electrode could be due to the effects of ZrO_2 nanoparticles on the ES-PANI peak intensity, which could also be caused by the interaction of oxygen (related to ZrO_2) and hydrogen of the N-H group of the ES-PANI polymer chain [60], [64]. These results are supported by the results of FTIR analysis of materials and the presence of functional groups in Figure 5.

3.5. Elemental analysis

Figure 7 and Figure 8 display the EDX spectrum and the elemental mapping with the SEM image of the E2 composite electrode. The presence of the C, O, and N elements can be related to the oxide, carboxylic, and nitrogenous functional groups, according to the results of the FTIR analysis. The presence of chloride and fluoride elements in Figure 7 is due to PVDF and ES-PANI in the preparation of the electrode. The percentage of elements in the subset table of Figure 7 confirms the successful incorporation of the components of the composite electrode. In Figure 8, the mapping of key elements such as C, N, O, and Zr and their amounts imply the good distribution of materials in the structure of the composite electrode.

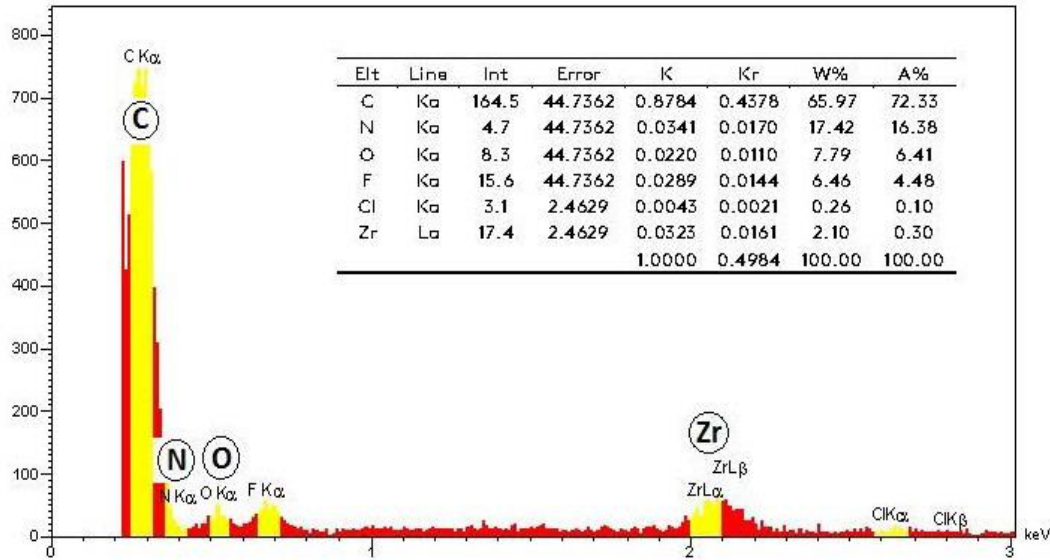


Fig. 7. EDS spectra of E2 composite electrode.

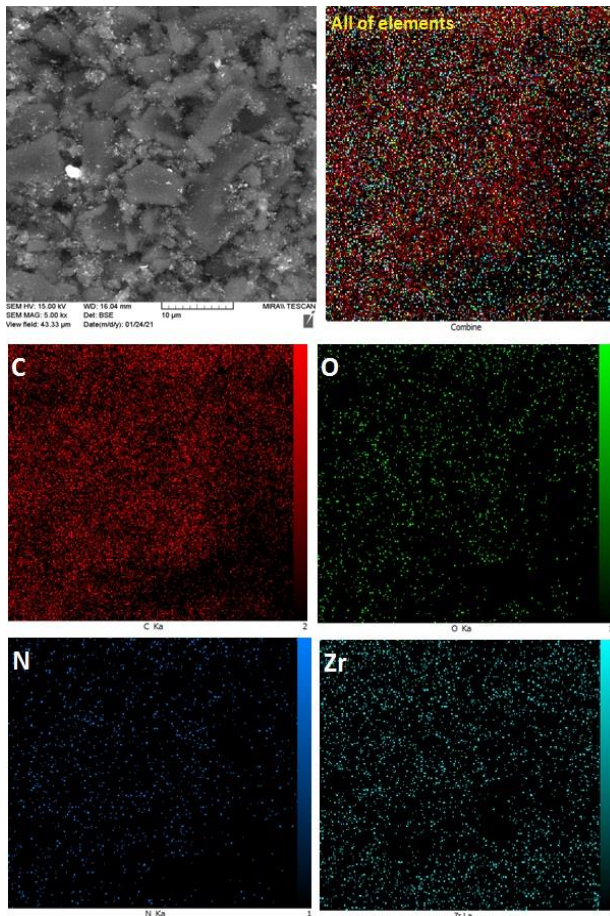


Fig. 8. Elemental mapping of C, O, N, and Zr in the E2 composite electrode.

3.6. Electrochemical evaluations

Based on Figure 9, in the cyclic voltammetry action of the E1 and E2 electrodes, pseudo-capacitive behaviors were demonstrated for both electrodes as well as the higher specific capacitance of the E2 than the E1 electrode [22]. Increasing the 41.8% increment in the specific capacitance of the E2 electrode ($C_{s,E1} = 52.51 \text{ F/g}$ and $C_{s,E2} = 90.24 \text{ F/g}$) can be related to several parameters of the composite electrode such as the good interaction of ions and existing functional groups of the electrode (i.e., carboxyl, hydroxyl, and amine), improved wettability, low electrical resistance, or improved conductivity, which refer to the presence of PANI and ZrO_2 in the AC matrix [28], [66]. Nyquist plots of the electrodes using the EIS test are shown in Fig. 10. In comparing these diagrams, it is evident that the diameter of the cyclic voltammetry plot of the E2 electrode and its intersection with the X-axis is lower than that of the E1 electrode. This trend returns to the decreased electrical resistivity of the E2 electrode as a result of the addition of 6% PANI-ES to AC [61] and faster interfacial charge transfer as a consequence of hydrophilic nature as well as mesoporous structures of existing ZrO_2 in the E2 electrode [65]. Finally, the incorporation of either PANI-ES or the existing ZrO_2 in the E2 electrode led

to about a 29.2% decrement of ion charge transfer resistance relative to that of the E1 electrode.

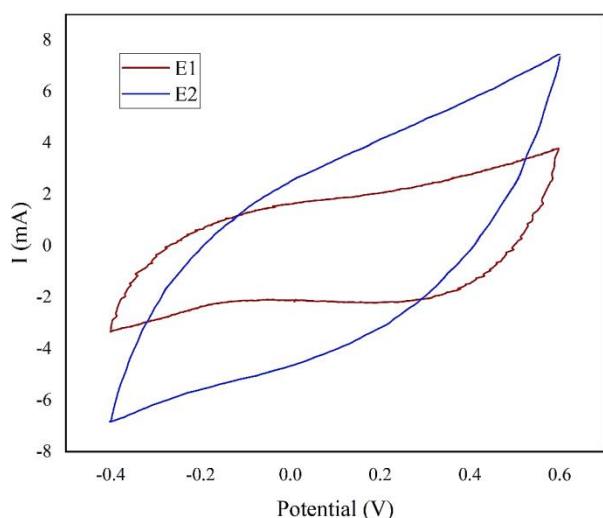


Fig. 9. Cyclic voltammery of E1 and E2 electrodes at scan rate of 10 mV/s in 0.5 M NaNO₃.

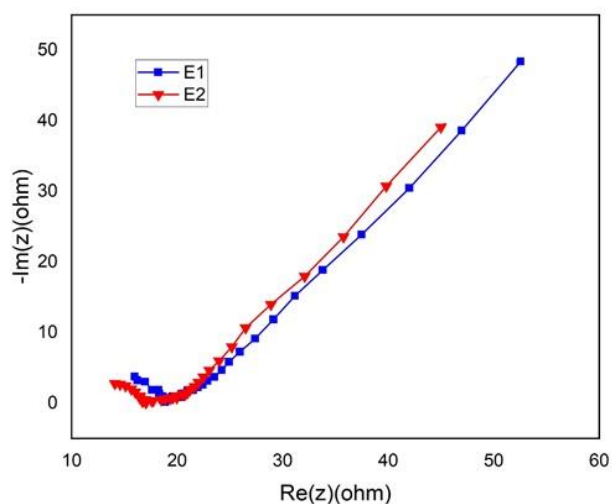


Fig. 10. The resistance of ion charge transfer of the E1 and E2 electrodes by Nyquist plots (at the frequency range of 100.0 kHz to 10.0 mHz and the alternating voltage amplitude of 10.0 mV).

3.7. CDI and MCDI performance by the composite electrode

Fig. 11 illustrates the conductivity variations of the outlet stream for the two cells at an applied potential of 2.0 V with the feed concentration of 100 mg/L for each of NaCl and NaNO₃ by the E1 and E2 electrodes. When the working potential of 2.0 V was used for the electrosorption step, decreasing of the solution conductivity rapidly occurred by MCDI in 30 min, while it took 65 min in the CDI process based on the E2 electrode. Furthermore, as seen in

Fig. 11, when the MCDI starts its adsorption process, the conductivity of the outlet stream decreases sharply from 307.2 $\mu\text{S}/\text{cm}$ to 221.5 $\mu\text{S}/\text{cm}$ for E2 and from 307.2 $\mu\text{S}/\text{cm}$ to 272.3 $\mu\text{S}/\text{cm}$ for E1 at the start and at that point remains consistent. However, similar trend was happened with a smaller variation in conductivity of E1 and E2 electrodes in the CDI process. On the other hand, during the MCDI process, the synergistic role of the E2 electrode and the ion-selective membrane causes greater separation of the nitrate ions than the performance of E1. The reduced conductivity in the MCDI process is related to the blocked co-ions by the IEM [33]. Li et al. (2019) [66] and Lee et al. (2011) reported similar results to those of this study for CDI and MCDI performance [39]. Usually, the slope of decreasing conductivity is greater at the beginning of the separation process because of the formation of an electrical-double layer (EDL) in the electrode-electrolyte interface, the presence of strong electrostatic attraction force, and the existence of accessible active sites of mesopores and micropores in the electrode structure. It is noted that the electrical-double layer capacitance of porous carbon electrodes is extremely related to its pore size distribution [67]. Accordingly, it can be observed that in the adsorption step, a rapid decrease of conductivity occurs for both CDI and MCDI cells due to the migration of ions from the solution to the E2 electrode compared with E1. It is due to the presence of more mesopores and lower electrical resistance (because of improved wettability) to ionic charge transfer in the E2 electrode. Therefore, improving the electrical conductivity and wettability properties of the E2 electrode leads to accessing more active sites of mesopores and micropores in the carbon electrode matrix for ion absorption. It can be related to the synergistic effect of ZrO₂ and ES- PANi because of the presence of hydrophilic, oxygen, and nitrogen functional groups on the carbon composite electrode [45], [57]. Also, the hydration ratio has been considered an important factor for ion selectivity than the hydrated radius. NO₃⁻ with a hydration ratio of 1.27 compared with the Cl⁻ hydration ratio of 1.83 has a smaller hydration ratio, which tends to have a higher selectivity of nitrate ions in the CDI process [33]. Indeed, nitrate ions with a smaller hydration ratio reveal a stronger

electrostatic attraction with the carbon electrode in CDI [70-71]. On the other hand, the chemical interaction between the ions and the carbon electrode surface can also determine the electrosorption affinity of NO_3^- compared with Cl^- in the CDI process [71-72]. Therefore, according to the adsorption process experiments, the basic oxygen functional groups on AC materials have been evaluated as possible attraction sites for NO_3^- [70]. According to Eqs. (2) and (3), the nitrate electrosorption capacity and the ion removal efficiency were 7.51 mg/g and 81.06% for MCDI, while those parameters were 5.81 mg/g and 56.49% for CDI process based on the E2 electrode. Also, those parameters were 2.34 mg/g (40.18%) and 1.51 mg/g (26.01%) for the E1 electrode in MCDI and CDI, respectively. As shown in Figure 12, the results indicate that the E2 electrode performance in the amount of electrosorption capacity and the ion removal efficiency evaluated 50% higher than the E1 electrode performance during the CDI and MCDI processes.

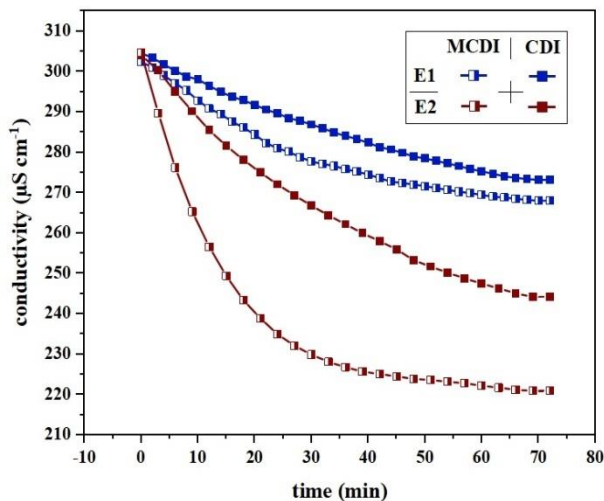


Fig. 11. Comparison of conductivity changes in a mixed solution under applied voltage 2.0 volt, flow rate of 10 mL/min, and solution volume of 200mL by MCDI and CDI processes based on the E1 and E2 electrodes.

On the other hand, as shown in Table 3, the capacity of the adsorbed nitrate ion in the MCDI process was 30.34% higher than the CDI process by the E2 electrode. In addition, the nitrate ions' selectivity compared to the chloride ions according to Equation (4) are listed in Table 4. These results show that the nitrate ion selectivity of E2 improved by approximately 45.95% compared with E1 in CDI, while this factor increased about 20.45% for E2

compared to E1 in the MCDI process. Thus, the role of the composite electrode has been extremely effective.

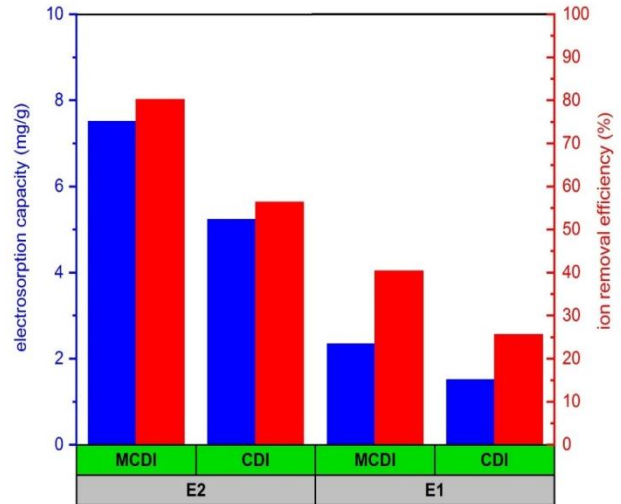


Fig. 12. Comparison of electrosorption capacity and the ion removal efficiency by MCDI and CDI processes based on the E1 and E2 electrodes.

Table 3. The amount of each ion adsorbed by the CDI and MCDI(AEM) processes are based on the E2 electrode.

Ion	The amount of ion adsorbed(mg/g)		The ion removal efficiency (%)	
	CDI process	MCDI process	CDI process	MCDI process
Cl^-	2.74	1.12	23.82	9.72
NO_3^-	5.23	7.51	56.49	81.06
Na^+	5.81	2.91	38.38	19.25

Table 4. The amount of each ion adsorbed by the E2 electrode in the CDI and MCDI (AEM) processes.

Process	E2	E1
CDI	2.37	1.33
MCDI	4.83	4.01

It is observed that the existence of the anion-exchange membrane (AEM) is too beneficial for the electrosorption of nitrate ions due to the fast transfer of counter-ions, therefore, obstructing the co-ions. And it is confirmed by the steeper slope of the adsorption curve for MCDI in Figure 11. Hence, the enhancement of the performance of the MCDI process in comparison to the CDI process under similar conditions is dependent on the selectivity of the AEM [33]. However, irrespective of the type of AEM used, the presence of hydrophilic, imine, and amine functional groups in the structure of the composite electrode plays a vital role in removing nitrate ions from the feed solution [70]. According

to the reported data on ion adsorption capacity and nitrate ion removal efficiency of activated carbon-based (AC) electrodes, the performance of the composite electrode and other electrodes with the new materials is presented in Table 5. As seen in Table 5, the results demonstrate that the nitrate ion capacity and adsorbed efficiency for the E2 electrode were about 15.86% and 15.02 %, which

are higher than those in (73). Also, a comparison of ion removal efficiency between this work and the studies of (37) and (75) found an improvement of about 28.44% and 33.60 %, respectively. Therefore, the results indicate that the electrode performance with more efficiency can be considered a promising alternative composite electrode to separate nitrate ions from water.

Table 5. Comparison of the electrosorption capacities and the removal efficiency of some AC electrodes for nitrate ions.

Type of electrode	Process	Applied voltage (V)	Flow rate (mL/min)	Initial nitrate concentration (mg/L)	Removal efficiency (%)	Electrosorption capacity (mg/g)	Reference
AC(10%PVDF)	CDI/BM	1	50	125	-	3.1	[34]
AC(35% self-made binder)	CDI/BM	1.2	-	125	77	5.5	[71]
Pd/NiAl-LMO	CDI/BM	1	-	100	40.47	-	[32]
AC/carbon black/PVDF	CDI/SP	1.4	10	220	73.48	4.5	[72]
AC/GP with A520E resin (in reactor2)	MCDI/BM	1.0	15	62.5	53.82	-	[73]
AC/PVDF	CDI/SP	1.2	2	70	48	5.5	[74]
AC/ PVDF with AEM	MCDI/BM	1.6	50	125	58	-	[35]
AC/PVDF/ZrO ₂ /PANi	CDI/BM	2.0	10	45.62	56.49	5.23	This study
AC/PVDF/ZrO ₂ /PANi with FAB-PK-130	MCDI/BM	2	10	45.62	81.06	7.51	This study

SP / single-pass, BM / batch-mode, η_i / ion removal efficiency, E_c / electrosorption capacity.

4. Conclusions

This study evaluated the adsorption of nitrate from binary salt feed via CDI and MCDI processes using a new composite electrode made up of AC, PVDF, ZrO₂, and PANi materials. To synthesize the composite electrode, it was necessary to incorporate the correct percentage of materials to make the electrode. so, the experimental design was applied by the mixture design technique to obtain suitable composition of the electrodes. On the other hand, the presence of PANi and ZrO₂ materials in the electrode structure enhanced the electrical conductivity, wettability, and nitrate ions adsorption capacity. The results showed that the final nitrate ions adsorption capacity was 7.51 mg/g and 5.23 mg/g for CDI and MCDI processes in a batch system, respectively. Moreover, the results indicated that the adsorbed nitrate ion in the MCDI process was higher than 30.34% compared to the CDI process by the composite electrode. Also,

electrode E2, compared to electrode E1, improved the performance by almost 50% in the amount of adsorbed nitrate ion and ion adsorption efficiency during the CDI and MCDI processes. This performance improvement of the E2 electrode was due to the formation of main mesopores and the presence of functional groups in the structure of electrode E2 because of the synergistic role of ZrO₂ and PANi. The enhancement of the performance of the MCDI process in comparison with the CDI process was dependent on AEM, and from a practical point of view, the E2 electrode demonstrated a good performance during the separation process to remove nitrate ions. In fact, the obtained results for both processes well illustrated the role of the composite electrode to adsorb nitrate ions in competition with the chloride ions. As mentioned, this action could be due to the presence of hydrophilic and amine functional groups, as well as electrical properties in the structure of the composite electrode that perform

a significant role in the adsorption of nitrate ions. In brief, this study attempted to develop high-efficiency electrode materials for use in the separation field to remove nitrate ions from water.

References

- [1] Tang, K., Kim, Y. H., Chang, J., Mayes, R. T., Gabitto, J., Yiacoumi, S., Tsouris, C. (2019). Seawater desalination by over-potential membrane capacitive deionization: Opportunities and hurdles. *Chemical engineering journal*, 357, 103-111.
- [2] Tang, W., Kovalsky, P., He, D., Waite, T. D. (2015). Fluoride and nitrate removal from brackish groundwaters by batch-mode capacitive deionization. *Water research*, 84, 342-349.
- [3] Zuo, K., Kim, J., Jain, A., Wang, T., Verduzco, R., Long, M., Li, Q. (2018). Novel composite electrodes for selective removal of sulfate by the capacitive deionization process. *Environmental science and technology*, 52(16), 9486-9494.
- [4] Chen, R., Sheehan, T., Ng, J. L., Brucks, M., Su, X. (2020). Capacitive deionization and electrosorption for heavy metal removal. *Environmental science: Water research and technology*, 6(2), 258-282.
- [5] Seo, S. J., Jeon, H., Lee, J. K., Kim, G. Y., Park, D., Nojima, H., Moon, S. H. (2010). Investigation on removal of hardness ions by capacitive deionization (CDI) for water softening applications. *Water research*, 44(7), 2267-2275.
- [6] Xing, W., Liang, J., Tang, W., Zeng, G., Wang, X., Li, X., Huang, M. (2019). Perchlorate removal from brackish water by capacitive deionization: Experimental and theoretical investigations. *Chemical engineering journal*, 361, 209-218.
- [7] Oren, Y. (2008). Capacitive deionization (CDI) for desalination and water treatment—past, present and future (a review). *Desalination*, 228(1-3), 10-29.
- [8] Zhao, Y., Wang, Y., Wang, R., Wu, Y., Xu, S., Wang, J. (2013). Performance comparison and energy consumption analysis of capacitive deionization and membrane capacitive deionization processes. *Desalination*, 324, 127-133.
- [9] Wang, C., Song, H., Zhang, Q., Wang, B., Li, A. (2015). Parameter optimization based on capacitive deionization for highly efficient desalination of domestic wastewater biotreated effluent and the fouled electrode regeneration. *Desalination*, 365, 407-415.
- [10] Anderson, M. A., Cudero, A. L., Palma, J. (2010). Capacitive deionization as an electrochemical means of saving energy and delivering clean water. Comparison to present desalination practices: Will it compete?. *Electrochimica acta*, 55(12), 3845-3856.
- [11] Seed, L. P., Yetman, D. D., Pargaru, Y., Shelp, G. S. (2006). The DesEL system—capacitive deionization for the removal of ions from water. *Proceedings of the water environment federation*, 2006(5), 7172-7180.
- [12] Liu, N. L., Sun, S. H., Hou, C. H. (2019). Studying the electrosorption performance of activated carbon electrodes in batch-mode and single-pass capacitive deionization. *Separation and purification technology*, 215, 403-409.
- [13] Md, A., Ahmed, S. (2018). Tewari, Capacitive deionization: Processes, materials and state of the technology. *Journal of. electroanal chemistry*, 813, 178-192.
- [14] Mossad, M., Zou, L. (2012). A study of the capacitive deionisation performance under various operational conditions. *Journal of hazardous materials*, 213, 491-497.
- [15] McNair, R., Szekely, G., Dryfe, R. A. (2020). Ion-exchange materials for membrane capacitive deionization. *ACS ES and T Water*, 1(2), 217-239.
- [16] Hassanvand, A., Chen, G. Q., Webley, P. A., & Kentish, S. E. (2018). A comparison of multicomponent electrosorption in capacitive deionization and membrane capacitive deionization. *Water research*, 131, 100-109.
- [17] Yan, T., Xu, B., Zhang, J., Shi, L., Zhang, D. (2018). Ion-selective asymmetric carbon electrodes for enhanced capacitive deionization. *SC advances*, 8(5), 2490-2497.
- [18] Yasin, A. S., Mohamed, A. Y., Mohamed, I. M., Cho, D. Y., Park, C. H., Kim, C. S. (2019). Theoretical insight into the structure-property relationship of mixed transition metal oxides nanofibers doped in activated carbon and 3D

- graphene for capacitive deionization. *Chemical engineering journal*, 371, 166-181.
- [19] Chung, S., Kang, H., Ocon, J. D., Lee, J. K., Lee, J. (2015). Enhanced electrical and mass transfer characteristics of acid-treated carbon nanotubes for capacitive deionization. *Current applied physics*, 15(11), 1539-1544.
- [20] Jia, B., Zhang, W. (2016). Preparation and application of electrodes in capacitive deionization (CDI): a state-of-art review. *Nanoscale research letters*, 11(1), 1-25.
- [21] Sufiani, O., Tanaka, H., Teshima, K., Machunda, R. L., Jande, Y. A. (2020). Enhanced electrosorption capacity of activated carbon electrodes for deionized water production through capacitive deionization. *Separation and purification technology*, 247, 116998.
- [22] Zhang, C., Wang, X., Wang, H., Wu, X., Shen, J. (2019). A positive-negative alternate adsorption effect for capacitive deionization in nano-porous carbon aerogel electrodes to enhance desalination capacity. *Desalination*, 458, 45-53.
- [23] Kumar, R., Gupta, S. S., Katiyar, S., Raman, V. K., Varigala, S. K., Pradeep, T., Sharma, A. (2016). Carbon aerogels through organo-inorganic co-assembly and their application in water desalination by capacitive deionization. *Carbon*, 99, 375-383.
- [24] Feng, J., Xiong, S., Wang, Y. (2019). Atomic layer deposition of TiO₂ on carbon-nanotube membranes for enhanced capacitive deionization. *Separation and purification technology*, 213, 70-77.
- [25] Luo, G., Wang, Y., Gao, L., Zhang, D., Lin, T. (2018). Graphene bonded carbon nanofiber aerogels with high capacitive deionization capability. *Electrochimica acta*, 260, 656-663.
- [26] Ma, J., Wang, L., Yu, F. (2018). Water-enhanced performance in capacitive deionization for desalination based on graphene gel as electrode material. *Electrochimica acta*, 263, 40-46.
- [27] Liu, X., Chen, T., Qiao, W. C., Wang, Z., & Yu, L. (2017). Fabrication of graphene/activated carbon nanofiber composites for high performance capacitive deionization. *Journal of the Taiwan institute of chemical engineers*, 72, 213-219.
- [28] Yasin, A. S., Obaid, M., Mohamed, I. M., Yousef, A., Barakat, N. A. (2017). ZrO₂ nanofibers/activated carbon composite as a novel and effective electrode material for the enhancement of capacitive deionization performance. *RSC advances*, 7(8), 4616-4626.
- [29] Abi Jaoude, M., Alhseinat, E., Polychronopoulou, K., Bharath, G., Darawsheh, I. F. F., Anwer, S., Banat, F. (2020). Morphology-dependent electrochemical performance of MnO₂ nanostructures on graphene towards efficient capacitive deionization. *Electrochimica acta*, 330, 135202.
- [30] Hou, C. H., Liu, N. L., Hsu, H. L., Den, W. (2014). Development of multi-walled carbon nanotube/poly (vinyl alcohol) composite as electrode for capacitive deionization. *Separation and purification technology*, 130, 7-14.
- [31] Lado, J. J., Pérez-Roa, R. E., Wouters, J. J., Tejedor-Tejedor, M. I., Federspill, C., Ortiz, J. M., Anderson, M. A. (2017). Removal of nitrate by asymmetric capacitive deionization. *Separation and purification technology*, 183, 145-152.
- [32] Hu, C., Dong, J., Wang, T., Liu, R., Liu, H., Qu, J. (2018). Nitrate electro-sorption/reduction in capacitive deionization using a novel Pd/NiAl-layered metal oxide film electrode. *Chemical engineering journal*, 335, 475-482.
- [33] Tsai, S. W., Hackl, L., Kumar, A., Hou, C. H. (2021). Exploring the electrosorption selectivity of nitrate over chloride in capacitive deionization (CDI) and membrane capacitive deionization (MCDI). *Desalination*, 497, 114764.
- [34] Kim, Y. J., Kim, J. H., Choi, J. H. (2013). Selective removal of nitrate ions by controlling the applied current in membrane capacitive deionization (MCDI). *Journal of membrane science*, 429, 52-57.
- [35] Baghodrat, M., Mehri, F., Rowshanzamir, S. (2020). Electrochemical performance and enhanced nitrate removal of homogeneous polysulfone-based anion exchange membrane applied in membrane capacitive deionization cell. *Desalination*, 496, 114696.

- [36] Fatemina, R., Rowshanzamir, S., Mehri, F. (2021). Synergistically enhanced nitrate removal by capacitive deionization with activated carbon/PVDF/polyaniline/ZrO₂ composite electrode. *Separation and purification technology*, 274, 119108.
- [37] Kim, D. I., Gonzales, R. R., Dorji, P., Gwak, G., Phuntsho, S., Hong, S., Shon, H. (2020). Efficient recovery of nitrate from municipal wastewater via MCDI using anion-exchange polymer coated electrode embedded with nitrate selective resin. *Desalination*, 484, 114425.
- [38] Merle, G., Wessling, M., Nijmeijer, K. (2011). Anion exchange membranes for alkaline fuel cells: A review. *Journal of membrane science*, 377(1-2), 1-35.
- [39] Lee, J. Y., Seo, S. J., Yun, S. H., Moon, S. H. (2011). Preparation of ion exchanger layered electrodes for advanced membrane capacitive deionization (MCDI). *Water research*, 45(17), 5375-5380.
- [40] Min, X., Hu, X., Li, X., Wang, H., Yang, W. (2019). Synergistic effect of nitrogen, sulfur-codoping on porous carbon nanosheets as highly efficient electrodes for capacitive deionization. *Journal of colloid and Interface science*, 550, 147-158.
- [41] Li, Y., Chen, N., Li, Z., Shao, H., Qu, L. (2020). Frontiers of carbon materials as capacitive deionization electrodes. *Dalton transactions*, 49(16), 5006-5014.
- [42] Yeo, J. H., Choi, J. H. (2013). Enhancement of nitrate removal from a solution of mixed nitrate, chloride and sulfate ions using a nitrate-selective carbon electrode. *Desalination*, 320, 10-16.
- [43] Zengin, H., Kalaycı, G. (2010). Synthesis and characterization of polyaniline/activated carbon composites and preparation of conductive films. *Materials chemistry and physics*, 120(1), 46-53.
- [44] Magnuson, M., Guo, J. H., Butorin, S. M., Agui, A., Sâthe, C., Nordgren, J., Monkman, A. P. (1999). The electronic structure of polyaniline and doped phases studied by soft X-ray absorption and emission spectroscopies. *The journal of chemical physics*, 111(10), 4756-4761.
- [45] Bienkowski, K. (2006). Polyaniline and its derivatives doped with Lewis acids-synthesis and spectroscopic properties. Doctoral dissertation, Université Joseph-Fourier-Grenoble I; Warsaw University of Technology.
- [46] Li, H., Zou, L., Pan, L., Sun, Z. (2010). Novel graphene-like electrodes for capacitive deionization. *Environmental science and technology*, 44(22), 8692-8697.
- [47] Kim, J. S., Choi, J. H. (2010). Fabrication and characterization of a carbon electrode coated with cation-exchange polymer for the membrane capacitive deionization applications. *Journal of membrane science*, 355(1-2), 85-90.
- [48] Goel, P., Mandal, P., Bhuvanesh, E., Shahi, V. K., Chattopadhyay, S. (2021). Temperature resistant cross-linked brominated poly phenylene oxide-functionalized graphene oxide nanocomposite anion exchange membrane for desalination. *Separation and purification technology*, 255, 117730.
- [49] Xu, X., Pan, L., Liu, Y., Lu, T., Sun, Z. (2015). Enhanced capacitive deionization performance of graphene by nitrogen doping. *Journal of colloid and interface science*, 445, 143-150.
- [50] Alencherry, T., Naveen, A. R., Ghosh, S., Daniel, J., Venkataraghavan, R. (2017). Effect of increasing electrical conductivity and hydrophilicity on the electrosorption capacity of activated carbon electrodes for capacitive deionization. *Desalination*, 415, 14-19.
- [51] Zornitta, R. L., García-Mateos, F. J., Lado, J. J., Rodríguez-Mirasol, J., Cordero, T., Hammer, P., Ruotolo, L. A. (2017). High-performance activated carbon from polyaniline for capacitive deionization. *Carbon*, 123, 318-333.
- [52] Yasin, A. S., Mohamed, I., Mousa, H. M., Park, C. H., Kim, C. S. (2018). Facile synthesis of TiO₂/ZrO₂ nanofibers/nitrogen co-doped activated carbon to enhance the desalination and bacterial inactivation via capacitive deionization. *Scientific reports*, 8(1), 1-14.
- [53] Thommes, M. (2010). Physical adsorption characterization of nanoporous materials. *Chemie ingenieur technik*, 82(7), 1059-1073.
- [54] Porada, S., Zhao, R., Van Der Wal, A., Presser, V., Biesheuvel, P. M. (2013). Review on the science and technology of water desalination

- by capacitive deionization. *Progress in materials science*, 58(8), 1388-1442.
- [55] Prasanna, B. P., Avadhani, D. N., Muralidhara, H. B., Chaitra, K., Thomas, V. R., Revanasiddappa, M., Kathyayini, N. (2016). Synthesis of polyaniline/ZrO₂ nanocomposites and their performance in AC conductivity and electrochemical supercapacitance. *Bulletin of materials science*, 39(3), 667-675.
- [56] Abbas, Q., Pajak, D., Frąckowiak, E., Béguin, F. (2014). Effect of binder on the performance of carbon/carbon symmetric capacitors in salt aqueous electrolyte. *Electrochimica acta*, 140, 132-138.
- [57] Huang, W. E. I., Zhang, Y., Bao, S., Song, S. (2013). Desalination by capacitive deionization with carbon-based materials as electrode: a review. *Surface review and letters*, 20(06), 1330003.
- [58] Barbieri, O., Hahn, M., Herzog, A., Kötz, R. (2005). Capacitance limits of high surface area activated carbons for double layer capacitors. *Carbon*, 43(6), 1303-1310.
- [59] Ntakirutimana, S., Tan, W., Anderson, M. A., Wang, Y. (2020). Editors' Choice—Review—Activated carbon electrode design: Engineering tradeoff with respect to capacitive deionization performance. *Journal of the electrochemical society*, 167(14), 143501.
- [60] Tian, S., Zhang, Z., Zhang, X., Ostrikov, K. K. (2019). Capacitive deionization using commercial activated carbon fiber decorated with polyaniline. *Journal of colloid and interface science*, 537, 247-255.
- [61] Yan, C., Zou, L., Short, R. (2014). Polyaniline-modified activated carbon electrodes for capacitive deionization. *Desalination*, 333(1), 101-106.
- [62] Xu, G., Wang, N., Wei, J., Lv, L., Zhang, J., Chen, Z., Xu, Q. (2012). Preparation of graphene oxide/polyaniline nanocomposite with assistance of supercritical carbon dioxide for supercapacitor electrodes. *Industrial & engineering chemistry research*, 51(44), 14390-14398.
- [63] Srinivasan, P., Gottam, R. (2018). Infrared Spectra: Useful technique to identify the conductivity level of emeraldine form of polyaniline and indication of conductivity measurement either two or four probe technique. *Material. science. research. India*, 15(3), 2009-2017.
- [64] Shi, L., Wang, X., Lu, L., Yang, X., Wu, X. (2009). Preparation of TiO₂/polyaniline nanocomposite from a lyotropic liquid crystalline solution. *Synthetic Metals*, 159(23-24), 2525-2529.
- [65] Peng, Z., Zhang, D., Shi, L., Yan, T. (2012). High performance ordered mesoporous carbon/carbon nanotube composite electrodes for capacitive deionization. *Journal of materials chemistry*, 22(14), 6603-6612.
- [66] Li, G., Cai, W., Zhao, R., Hao, L. (2019). Electrosorptive removal of salt ions from water by membrane capacitive deionization (MCDI): characterization, adsorption equilibrium, and kinetics. *Environmental science and pollution research*, 26(17), 17787-17796.
- [67] Salitra, G., Soffer, A., Eliad, L., Cohen, Y., Aurbach, D. (2000). Carbon electrodes for double-layer capacitors I. Relations between ion and pore dimensions. *Journal of the electrochemical society*, 147(7), 2486.
- [68] Li, Y., Zhang, C., Jiang, Y., Wang, T. J., Wang, H. (2016). Effects of the hydration ratio on the electrosorption selectivity of ions during capacitive deionization. *Desalination*, 399, 171-177.
- [69] Mubita, T. M., Dykstra, J. E., Biesheuvel, P. M., Van Der Wal, A., Porada, S. (2019). Selective adsorption of nitrate over chloride in microporous carbons. *Water research*, 164, 114885.
- [70] Ota, K., Amano, Y., Aikawa, M., Machida, M. (2013). Removal of nitrate ions from water by activated carbons (ACs)—Influence of surface chemistry of ACs and coexisting chloride and sulfate ions. *Applied surface science*, 276, 838-842.
- [71] Tang, K., Kim, Y. H., Chang, J., Mayes, R. T., Gabitto, J., Yiacoumi, S., Tsouris, C. (2019). Seawater desalination by over-potential membrane capacitive deionization: Opportunities and hurdles. *Chemical engineering journal*, 357, 103-111.
- [72] Jiang, S., Wang, H., Xiong, G., Wang, X., Tan, S. (2018). Removal of nitrate using activated

carbon-based electrodes for capacitive deionization. *Water supply*, 18(6), 2028-2034.

[73] Gan, L., Wu, Y., Song, H., Zhang, S., Lu, C., Yang, S., Li, A. (2019). Selective removal of nitrate ion using a novel activated carbon composite carbon electrode in capacitive

deionization. *Separation and purification technology*, 212, 728-736.

[74] Pastushok, O., Zhao, F., Ramasamy, D. L., Sillanpää, M. (2019). Nitrate removal and recovery by capacitive deionization (CDI). *Chemical engineering journal*, 375, 121943.